

Metal-Free Flat Lens Using Negative Refraction by Nonlinear Four-Wave Mixing

Jianjun Cao,¹ Yuanlin Zheng,¹ Yaming Feng,¹ Xianfeng Chen,^{1,3} and Wenjie Wan^{1,2,3,*}

¹The State Key Laboratory of Advanced Optical Communication Systems and Networks,

Department of Physics and Astronomy, Shanghai Jiao Tong University, Shanghai 200240, China

²University of Michigan-Shanghai Jiao Tong University Joint Institute, Shanghai Jiao Tong University, Shanghai 200240, China

³Key Laboratory for Laser Plasmas (Ministry of Education), Shanghai Jiao Tong University, Shanghai 200240, China

(Received 20 May 2014; revised manuscript received 12 September 2014; published 17 November 2014)

A perfect lens with unlimited resolution has always posed a challenge to both theoretical and experimental physicists. Recent developments in optical metamaterials promise an attractive approach towards perfect lenses using negative refraction to overcome the diffraction limit, improving resolution. However, those artificially engineered metamaterials are usually accompanied by high losses from metals and are extremely difficult to fabricate. An alternative proposal using negative refraction by four-wave mixing has attracted much interest recently, though most existing experiments still require metals and none of them have been implemented for an optical lens. Here, we experimentally demonstrate a metal-free flat lens for the first time using negative refraction by degenerate four-wave mixing with a thin glass slide. We realize an optical lensing effect utilizing a nonlinear refraction law, which may have potential applications in microscopy.

DOI: 10.1103/PhysRevLett.113.217401

PACS numbers: 78.66.Jg, 42.30.-d, 42.65.-k, 78.20.Ci

Flat lenses using negative refraction create a new avenue for novel optical imaging applications, attracting intense interest from the optics, microwave, and even acoustic communities [1–7]. Unlike traditional optical lenses, a flat lens which can bend incoming waves at negative angles opposed to those within the normal refraction regime [1–3] can form an image much more sharply thanks to its ability to negatively refract waves at all angles including evanescent ones, making it a “perfect lens” to overcome the diffraction limit [2,6]. Such lenses have been realized in many formats ranging from optics and microwave to acoustic, including photonic crystals [7], metal thin films [6], metamaterials [5,8–11], etc. However, most of them suffer from high losses in association with metallic materials, which are the key elements bringing in negative permittivity and artificial permeability. Second, fabrications of such nano- or microstructures raise additional obstacles for their practical applications. In nonlinear optics, alternative approaches to achieve negative refraction have been proposed, including phase conjugation, time reversal, and four-wave mixing (4WM) [3,12,13]. In contrast to those artificially engineered methods, i.e., metamaterials and photonic crystals, which create spatial dispersion for negative refraction using the linear composition of different materials, nonlinear optics explores nonlinear wave mixings with angle matching schemes to fulfill the requirements for negative refraction. Principally, only a thin flat nonlinear slab is required. Up to now, such negative refractions using wave mixing have been realized in some thin films with high nonlinearity such as metal and graphite thin films [14–16]. However, in these experiments, due to their low nonlinear conversion efficiencies or

their materials’ optical transparency, none of them have been implemented for imaging purposes.

In this Letter, we experimentally demonstrate a metal-free flat lens using negative refraction by degenerate four-wave mixing with a simple thin glass slide. Within glass slides containing third-order nonlinearity, a multi-color imaging scheme is realized at the millimeter scale by converting the original infrared beams into negative refracted visible ones through nonlinear wave mixings. During degenerate four-wave mixing processes, the phase matching conditions enable the negative refraction of 4WM beams as opposed to probe beams at some special angles. These negatively refracted 4WM beams can focus and form images while slight phase mismatches due to dispersion effects or slabs’ thicknesses can blur images. In order to enhance the resolution of images, we study both collinear and noncollinear configurations aiming to increase numerical apertures. This new imaging technique may offer a new platform for novel microscopy applications in the near future.

In a degenerate 4WM scheme, an intense pump beam at frequency ω_1 and a probe beam at frequency ω_2 are incident onto a slab with third-order nonlinear susceptibility $\chi^{(3)}$, generating a 4WM wave at frequency $\omega_3 = 2\omega_1 - \omega_2$. Their corresponding phases should satisfy the phase matching condition $k_3 = 2k_1 - k_2$ to ensure efficient wavelength conversion. With a thin slab material, its thickness can also affect 4WM processes, allowing 4WM with slightly mismatched phases [17]. Moreover, if the slab’s thickness is shorter than the wavelength, only partial phase matching is required in nonlinear surface plasmon excitations [14,18,19] or nonlinear dark-field microscopes [20]. In our experiment, the pump beam at

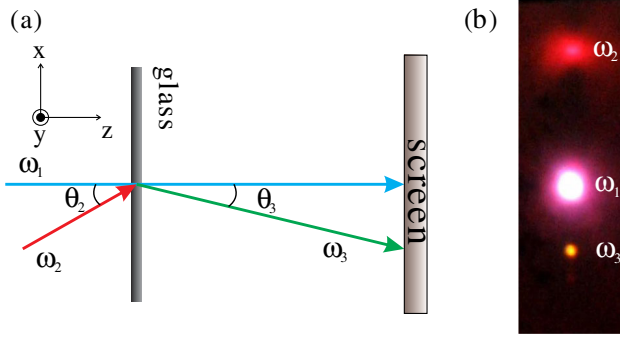


FIG. 1 (color online). (a) Schematic of the negative refraction effect by degenerate 4WM in a planar glass slide. The pump beam at frequency ω_1 is incident normally on the glass slide mixing with the probe beam at frequency ω_2 to generate the 4WM wave at a frequency $2\omega_1 - \omega_2$. The 4WM beam exhibits negative refraction as opposed to the probe beam. (b) Color image on the IR viewing card. The transmitted probe beam at $\lambda_2 = 1300$ nm and the generated 4WM beam at $\lambda_3 = 578$ nm are located on the opposite sides of the screen.

ω_1 is incident on a thin glass slide normally and the probe beam at ω_2 (signal beam carrying the original image) is incident at the angle of θ_2 , as shown in Fig. 1(a). The angle of the generated 4WM wave is denoted as θ_3 , measured with respect to the surface normal in the counterclockwise direction, which is negatively opposed to the normal refraction condition through a thin glass. The phase mismatch of the 4WM process reads

$$\Delta k = 2k_1 - k_2 - k_3, \quad (1)$$

where $k_i = 2\pi n_i/\lambda_i$ ($i = 1, 2, 3$) are the wave vectors of the pump, the probe, and the 4WM beam, respectively. The n_i are the corresponding refractive indices of the medium. To generate an efficient 4WM wave, the phase matching condition should be satisfied; i.e., $\Delta k = 0$, which leads to

$$2k_1 = k_2 \cos \theta_2^m + k_3 \cos \theta_3^m, \quad (2)$$

$$k_2 \sin \theta_2^m = -k_3 \sin \theta_3^m, \quad (3)$$

where θ_2^m and θ_3^m are the angles in the medium. These two angles are related to the angles in air by Snell's law:

$$\sin \theta_2 = n_2 \sin \theta_2^m, \quad (4)$$

$$\sin \theta_3 = n_3 \sin \theta_3^m. \quad (5)$$

Equation (3) indicates that the 4WM wave is refracted negatively with respect to the incident probe beam. Inserting Eqs. (4) and (5) into Eq. (3), a Snell-like nonlinear refraction law is obtained [14]:

$$\frac{\sin \theta_2}{\sin \theta_3} = -\frac{\lambda_2}{\lambda_3}. \quad (6)$$

In our experiments, the pump beam is delivered by a Ti:sapphire femtosecond laser source with the pulse duration of ~ 75 fs and central wavelength $\lambda_1 = 800$ nm. An optical parametric amplifier provides pulses of similar duration at wavelength $\lambda_2 = 1300$ nm as the probe beam. A 1 mm thick BK7 glass slide is used as the nonlinear material. The laser beams are incident on the glass slide using the geometry in Fig. 1(a), and a delay line is added to ensure the pulses' time overlapping. The generated 4WM waves after the beams passing through the glass slide are shown in Fig. 1(b). Obviously, the generated 4WM beam is negatively refracted with respect to the input probe beam, located on the other side of the central pump beam's spot. The incident angle θ_2 is 7.9° , and the refracted angle θ_3 is -3.4° . By time delaying the probe beam, the 4WM intensity varies within a 165 fs time frame (see the Supplemental Material [21]), confirming that ω_3 is indeed generated by a nonlinear process. The polarization of the 4WM beam is also measured to be linearly polarized in the x direction, which is the same as the input beams. However, no particular polarization is required to generate 4WM waves due to the isotropic behaviors of $\chi^{(3)}$ about 2.8×10^{-22} m²/V² in BK7 glass [17], unlike the case in which surface plasmon wave excitation by 4WM only limits us to TM polarization [13,18,19]. The input powers of ω_1 and ω_2 are 34.5 and 10.3 mW. The power of the 4WM wave is 547 nW, corresponding to a conversion efficiency of 5×10^{-5} . Such a beam with 547 nW power is intense enough to be recorded by a visible CCD camera. The power of 4WM waves depends linearly on the probe beams (see the Supplemental Material [21]); meanwhile, the pump beams' power is limited to avoid any other nonlinear effects, e.g., self-focusing or thermal effects, that could potentially harm the nonlinear imaging quality. With the current configuration, we proceed to study the imaging formation using 4WM.

According to the nonlinear refraction law in Eq. (6), the refracted 4WM beam's angle linearly depends on its wavelength. Our experiment measurements confirm this linear relationship between $\sin \theta_2/\sin \theta_3$ and $-(\lambda_2/\lambda_3)$ to have a unit slope in Fig. 2(a) by varying the incident probe's wavelength from 1250 to 1500 nm while fixing the probe beam and the pump beam's angles. Such a nonlinear refraction law is the direct consequence of the phase matching condition in 4WM. As long as such a law holds, we may extend it to a wider band of probe wavelengths accepting larger angles (numerical apertures) for imaging purposes, enabling a better imaging resolution [20,22]. However, the phase matching scheme in our experiment is complicated by the ultrafast pulse's bandwidth and the glass slide's thickness. For example, although exact phase matching only allows 4WM waves to be generated at the

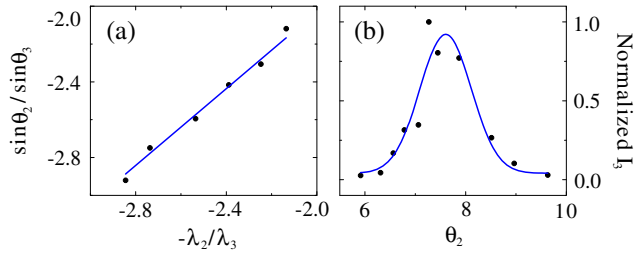


FIG. 2 (color online). (a) Nonlinear refraction law. The relationship between $\sin \theta_2 / \sin \theta_3$ and $-\lambda_2 / \lambda_3$ is plotted with the slope of 1.01 for the linear fitting. (b) The intensity of the 4WM wave as a function of the excitation angle θ_2 . The dots are measured 4WM intensities for the probe beam at wavelength $\lambda_2 = 1300$ nm. The solid curve is a Gaussian fitting.

exact angle, in real experiments, the ultrafast pulses have a finite linewidth ~ 50 nm for the pump and ~ 100 nm for the probe, allowing 4WMs to occur in a small angle spreading nearby. In Fig. 2(b), the 4WM intensity reaches its peak at $\theta_2 = 7.6^\circ$ close to the calculated value 7.2° by Eqs. (2) and (3), while the width of the peak spreads about $\Delta\theta_2 \approx 1.0^\circ$. Since the nonlinear refraction law in Eq. (6) depicts the linear dependence of wavelength λ to $\sin \theta$, this angle spreading is roughly close to $\sim 0.91^\circ$ spreading, calculated accordingly with the input beams' linewidth. However, for imaging applications, such small angle spreading can cause blurry images similar to chromatic aberrations due to the dispersion of a linear lens.

To experimentally realize a flat lens, we consider the phase matching condition in three-dimensional wave vector space, as shown in Fig. 3(a). The arrow ends of the incident wave vector k_2 that fulfill the phase matching condition in 3D compose a ring in the x - y plane. For the incident waves near the phase matching ring, their 4WM beams [green beam in Fig. 3(a)] can focus on the image side according to the nonlinear refraction law. However, for a particular incidence, e.g., k_2 in Fig. 3(a), the phase matching ring segment is not isotropic along the x - z and y - z planes; it allows a better phase matching along the y - z plane rather than the x - z plane in Fig. 3(b), enabling a better focus from multiple angled 4WM waves on the y - z plane. In contrast, on the x - z plane, only one exact phase matching angle is accepted to produce 4WM waves, giving a weak focus with poor image resolution.

First, we experimentally realize optical imaging in a noncollinear configuration as shown in Fig. 1(a), which explores the small angle cone spreading for 4WM near the phase matching ring mentioned above (see the Supplemental Material [21]). With such a configuration, the probe beam with a wavelength of 1300 nm is incident on the glass slice at the angle $\theta_2 = 7.8^\circ$ in the x - z plane while the pump beam maintains normal incidence. A USAF resolution card is placed in the path of the probe beam, 4.3 cm away from the glass slide. 4WM waves negatively refract and form the image on the other side of the glass

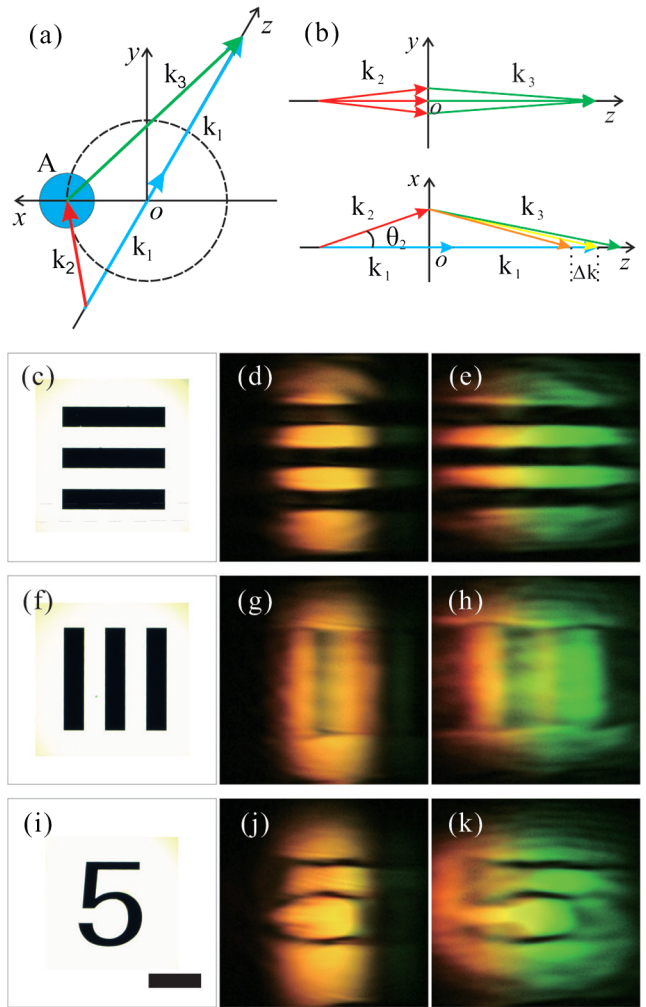


FIG. 3 (color online). Imaging a resolution card by the nonlinear negative refraction effect in the noncollinear configuration. (a) The phase matching condition for the degenerate 4WM process. Phase matching requires that $2k_1 - k_2 - k_3 = 0$. The dashed circular line indicates the end points of wave vector k_2 that fulfill the phase matching condition. The solid blue disk represents the Fourier plane image of the resolution card. (b) The phase matching triangles in the y - z plane and the x - z plane. (c),(f), (i) Input images of the resolution card. (d),(e),(g),(h),(j),(k) Measured images formed by the 4WM wave. The thickness of the glass slide is 1 mm for (d), (g), and (j) and 0.17 mm for (e), (h), and (k). The scale bar is $400 \mu\text{m}$.

slide. After filtering out the probe and pump beams with optical filters, we can obtain the sharpest image with a CCD camera near the focus point at the distance of around 9.0 cm away from the glass slide. By doing this, we achieve a flat lens by probing objects with one wavelength while forming images with others. Figures 3(c), 3(f), and 3(i) are input images of the resolution card, and Figs. 3(d), 3(g), and 3(j) are the corresponding images formed by 4WM waves. As a comparison, the image of horizontal lines is much clearer than those of vertical ones; this is because the small angle spreading caused by the object tends to have better phase

matching in the y - z plane, thanks to the phase matching ring along the y - z plane in Fig. 3(a), while in the x - z plane, such 4WM is less pronounced due to limited angles that allow for phase matching (the ring is a dot in the x - z plane, rather than a line in the y - z plane). Hence, 4WMs can be better generated and focused along the y - z plane, giving a finer resolution.

To investigate this effect further, we replace the glass slide with a thinner one of 0.17 mm thickness. Clearly, color images from Figs. 3(e), 3(h), and 3(k) show dispersive colors ranging from red to green. Also, we perform spectroscopic measurements along the horizontal axis with a thin vertical slit in front of the fiber cable of a spectrometer (see the Supplemental Material [21]) to confirm the angle spreading of the spectrum to be around 0.6° , almost twice that with the 1 mm thick glass slide. Here, the thickness of the thin glass slide provides an additional phase mismatching factor $\Delta k = 2\pi/d$ (d is the thickness) that allows $2k_1 - k_2 - k_3 - \Delta k = 0$; hence, a thinner lens leads to a wider phase matching angle in the x - z plane, as indicated in Fig. 3(b), similarly to the process in a surface plasmon excitation on a metal thin film [18,19]. Such phase mismatching leads to the extra angle spreading compared to the thick glass case in Figs. 3(d), 3(g), and 3(j), resulting in the enlarged field of view in the horizontal axis. Meanwhile, such a wider phase matching angle also enables multicolor 4WM generation, giving rise to the chromatic aberration illustrated in Fig. 3(b). Hence, image focusing in the x - z plane is complicated by this phase mismatching, leaving a poor resolution. It is also worth mentioning that (1) the image size is the same as the object (see Fig. 3), as these are one-to-one correspondences with mirror symmetry, with no magnification, and (2) the image distance Q is related to the object distance P by $Q/P = -(\tan \theta_2 / \tan \theta_3)$ (the segment in the x - y plane is the same).

In order to obtain a better resolution in the transverse plane, we construct a collinear configuration to access the full phase matching ring, where the pump and probe beams collinearly propagate, as shown in Fig. 4(a). The pump beam at $\lambda_1 = 800$ nm, reflected by a dichroic mirror (900 nm long pass), is incident on the glass slide normally. The probe beam at $\lambda_2 = 1350$ nm modulated by a “grating” is transformed and forms an “object” (as labeled in Fig. 4) in the front of the glass slide by a $4f$ system using two lenses with focal lengths of 4.5 and 6 cm, respectively, in order to avoid the pump beam. The image formed by the 4WM wave at $\lambda_3 = 568$ nm is recorded by a home-built microscope (see the Supplemental Material [21]). Unlike the noncollinear configuration, both the vertical and horizontal lines are clear in the current configuration by taking advantage of the phase matching around the full ring geometry in 3D vector space (Fig. 3). In such a way, we can obtain images for both the horizontal and vertical directions without the dispersion distortion as in the noncollinear configuration. However, these images seem to

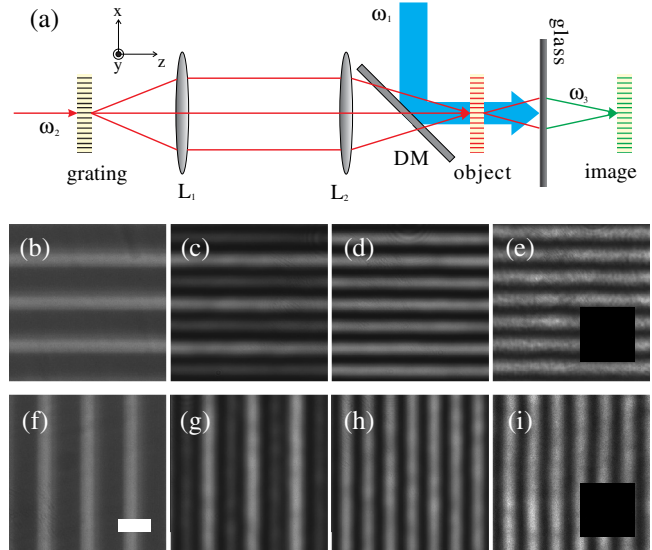


FIG. 4 (color online). Imaging a grating (object) by nonlinear negative refraction in a collinear configuration. (a) Experimental setup of the collinear configuration. L_1 , L_2 : lens; DM: dichroic mirror. (b),(f) Images of the object. (c),(g) Images of the object with grating orders ± 1 and 0. (d),(h) Images of the object with grating orders ± 1 only by blocking zero order; see the Supplemental Material [21]. (e),(i) Measured images formed by the 4WM waves. The insets show images without pump beams. The scale bar is $6.5 \mu\text{m}$.

have finer fringes [Figs. 4(e) and 4(i)] compared to the original object in Figs. 4(b) and 4(f); this is because 4WM only occurs around the phase matching ring while the probe beam with normal incidence cannot efficiently generate 4WM due to phase mismatching. Here, the object is formed by imaging the grating, which strongly diffracts the probe beam at 0, ± 1 orders. The ± 1 order diffractions are closer to the phase matching angles encouraging 4WM, while this is not the case for the zero-order one. Hence, 4WM images [Figs. 4(e) and 4(i)] are closer to those images of the grating by blocking zero-order diffraction [Figs. 4(d) and 4(h)] as opposed to those with it [Figs. 4(c) and 4(g)]; see the Supplemental Material [21]. The resolution of the image is determined by the input’s numerical aperture, the phase matching cone in our case, which can be estimated as $0.61\lambda_2 / \sin \theta_2 = 6 \mu\text{m}$, according to Abbe’s theory [23]. Since we detect images with a shorter wavelength, ideally, we could have a better resolution. Moreover, if combined with nonlinear numerical reconstruction methods in Refs. [24,25], the resolution can be improved further with an enlarged numerical aperture.

At last, we would like to comment on the direct implied applications with our flat lens. (1) Our flat lens can be applied in infrared (IR) microscopy. For those fluorescence dyes or biological tissues that emit IR light, our current configuration can convert them into visible light for better detection with a more sensitive visible CCD camera, e.g.,

EMCCD, with a simple glass slide. However, given the low nonlinear conversion efficiency in our current experiment, flat lenses with high nonlinearity will be studied in the future. (2) Compared with other flat lenses by a metal thin film [6] or photonic crystal [7,26], we can achieve a much larger image area up to the millimeter scale determined only by pump beam size. (3) Superresolution imaging is also possible by exploring a larger angle cone of the phase matching condition to accept the evanescent waves in order to break the diffraction limit; however, proper imaging reconstruction may be required; similar proposals have been proposed by using the plasmonic effect in metallic nanostructures [22,27].

This work was supported by the National Natural Science Foundation of China (Grants No. 11304201, No. 61125503 and No. 61235009), the National 1000-Plan Program (Youth), and the Shanghai Pujiang Talent Program (Grant No. 12PJ1404700).

*To whom all correspondence should be addressed.
wenjie.wan@sjtu.edu.cn

- [1] V. G. Veselago, *Sov. Phys. Usp.* **10**, 509 (1968).
- [2] J. B. Pendry, *Phys. Rev. Lett.* **85**, 3966 (2000).
- [3] J. B. Pendry, *Science* **322**, 71 (2008).
- [4] A. Grbic and G. V. Eleftheriades, *Phys. Rev. Lett.* **92**, 117403 (2004).
- [5] S. Zhang, L. L. Yin, and N. Fang, *Phys. Rev. Lett.* **102**, 194301 (2009).
- [6] N. Fang, H. Lee, C. Sun, and X. Zhang, *Science* **308**, 534 (2005).
- [7] P. V. Parimi, W. T. T. Lu, P. Vodo, and S. Sridhar, *Nature (London)* **426**, 404 (2003).
- [8] Z. W. Liu, H. Lee, Y. Xiong, C. Sun, and X. Zhang, *Science* **315**, 1686 (2007).
- [9] S. Zhang, W. J. Fan, N. C. Panoiu, K. J. Malloy, R. M. Osgood, and S. R. J. Brueck, *Phys. Rev. Lett.* **95**, 137404 (2005).
- [10] H. J. Lezec, J. A. Dionne, and H. A. Atwater, *Science* **316**, 430 (2007).
- [11] C. M. Soukoulis, S. Linden, and M. Wegener, *Science* **315**, 47 (2007).
- [12] S. Maslovski and S. Tretyakov, *J. Appl. Phys.* **94**, 4241 (2003).
- [13] A. Aubry and J. B. Pendry, *J. Opt. Soc. Am. B* **27**, 72 (2010).
- [14] S. Palomba, S. Zhang, Y. Park, G. Bartal, X. Yin, and X. Zhang, *Nat. Mater.* **11**, 34 (2011).
- [15] H. Harutyunyan, R. Beams, and L. Novotny, *Nat. Phys.* **9**, 423 (2013).
- [16] A. R. Katko, S. Gu, J. P. Barrett, B. I. Popa, G. Shvets, and S. A. Cummer, *Phys. Rev. Lett.* **105**, 123905 (2010).
- [17] R. W. Boyd, *Nonlinear Optics* (Academic, New York, 2008).
- [18] J. Renger, R. Quidant, N. van Hulst, S. Palomba, and L. Novotny, *Phys. Rev. Lett.* **103**, 266802 (2009).
- [19] J. Renger, R. Quidant, N. van Hulst, and L. Novotny, *Phys. Rev. Lett.* **104**, 046803 (2010).
- [20] H. Harutyunyan, S. Palomba, J. Renger, R. Quidant, and L. Novotny, *Nano Lett.* **10**, 5076 (2010).
- [21] See Supplemental Material at <http://link.aps.org/supplemental/10.1103/PhysRevLett.113.217401>, for details of pulse width, power dependence, polarization state and experimental setups.
- [22] B. Simkhovich and G. Bartal, *Phys. Rev. Lett.* **112**, 056802 (2014).
- [23] E. Abbe, *Arch. Mikrosk. Anat.* **9**, 413 (1873).
- [24] C. Barsi, W. J. Wan, and J. W. Fleischer, *Nat. Photonics* **3**, 211 (2009).
- [25] C. Barsi and J. W. Fleischer, *Nat. Photonics* **7**, 639 (2013).
- [26] N. Fabre, L. Lalouat, B. Cluzel, X. Melique, D. Lippens, F. de Fornel, and O. Vanbesien, *Phys. Rev. Lett.* **101**, 073901 (2008).
- [27] P. Y. Chen and A. Alu, *Nano Lett.* **11**, 5514 (2011).